NANO LETTERS

Letter

pubs.acs.org/NanoLett

General Thermal Texturization Process of MoS_2 for Efficient Electrocatalytic Hydrogen Evolution Reaction

Daisuke Kiriya,[†,§,∥] Peter Lobaccaro,[‡,∥,⊥] Hnin Yin Yin Nyein,[†,§,∥] Peyman Taheri,[†,∥] Mark Hettick,[†,§,∥,⊥] Hiroshi Shiraki,[†,§,∥] Carolin M. Sutter-Fella,[†,§,∥] Peida Zhao,[†,§,∥] Wei Gao,[†,§,∥] Roya Maboudian,[‡,∥] Joel W. Ager,[§,⊥] and Ali Javey*[,†,§,∥]

[†]Department of Electrical Engineering and Computer Sciences, University of California at Berkeley, Berkeley, California 94720, United States

[‡]Department of Chemical and Biomolecular Engineering, University of California at Berkeley, Berkeley, California 94720, United States

[§]Materials Sciences Division, Lawrence Berkeley National Laboratory, Berkeley, California 94720, United States

[∥]Berkeley Sensor & Actuator Center, University of California, Berkeley, California 94720, United States

[⊥]Joint Center for Artificial Photosynthesis, Lawrence Berkeley National Laboratory, Berkeley, California 94720, United States

Supporting Information

ABSTRACT: Molybdenum disulfide (MoS_2) has been widely examined as a catalyst containing no precious metals for the hydrogen evolution reaction (HER); however, these examinations have utilized synthesized MoS_2 because the pristine MoS_2 mineral is known to be a poor catalyst. The fundamental challenge with pristine MoS_2 is the inert HER activity of the predominant (0001) basal surface plane. In order to achieve high HER performance with pristine MoS_2, it is essential to activate the basal plane. Here, we report a general thermal process in which the basal plane is texturized to increase the density of HER-active edge sites. This texturization is achieved through a simple thermal annealing procedure in a hydrogen environment, removing sulfur from the MoS_2 surface to form edge sites. As a result, the process generates high HER catalytic performance in pristine MoS_2 across various morphologies such as the bulk mineral, films composed of micron-scale flakes, and even films of a commercially available spray of nanoflake MoS_2. The lowest overpotential (η) observed for these samples was η = 170 mV to obtain 10 mA/cm^2 of HER current density.

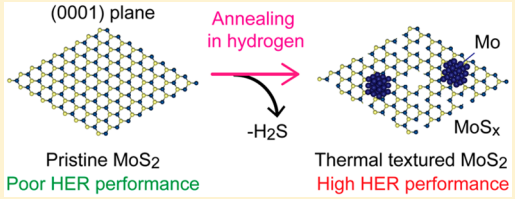

KEYWORDS: *MoS_2, edge site, hydrogen evolution reaction, thermal texturization, hydrogen thermal processing*

Renewable energy sources such as wind and solar have shown great promise in the past decade; however, the issue of their intermittency, and thus the need for energy storage, remains unsolved.[1] Energy storage via chemical fuels is highly desirable due to their high energy densities, and while hydrocarbon based liquid fuels remain the most desirable, hydrogen presents an attractive alternative. Hydrogen production via electrochemical water splitting, specifically the hydrogen evolution reaction (HER), has been widely studied[2−6] and has inspired a vision of a hydrogen powered economy.[7,8] This goal has stimulated a large portfolio of research in catalysts to reduce the overpotential required by the HER. MoS_2 has emerged as a promising catalyst for HER because it is earth-abundant, cheap, and chemically stable.[9−11] Although bulk MoS_2 (i.e., the pristine mineral) is not an active HER catalyst, it is known that exposed MoS_2 edge sites act as highly active catalytic sites.[12−14] For this reason various MoS_2 HER catalysts have been synthesized via solution-based or vapor-based methods, which effectively maximize the density of edge sites through synthesizing nanosized flakes,[15,16] porous structures,[17,18] or vertically aligned structures.[19−21] However, if the pristine MoS_2 mineral could be converted into an efficient catalyst, which is the basic structure of all MoS_2 morphologies, a wide array of MoS_2 starting materials could be converted into HER catalysts. In order to achieve this, pristine MoS_2 needs to overcome several fundamental issues to increase its catalytic activity. First, the (0001) plane is dominant in the pristine MoS_2 mineral which is an inactive plane for HER.[12,17] Second, pristine MoS_2 is predominately of the 2H crystal phase which exhibits poor conductivity.[22−24] These issues generally eliminate pristine bulk MoS_2 as an electrochemical HER catalyst.

Here, we demonstrate a general thermal texturization procedure which can convert bulk MoS_2 of many morphologies into a HER catalyst. Bulk mineral MoS_2, micron-scale commercial MoS_2 powders, and even a commercially available, nanoflake MoS_2 based lubricant spray, all of which showed poor HER activity before treatment, show high HER performance after thermal texturization. We found that annealing in a hydrogen environment increases the surface area and reduces

Received: February 9, 2016
Revised: May 27, 2016

DOI: 10.1021/acs.nanolett.6b00569
Nano Lett. XXXX, XXX, XXX−XXX

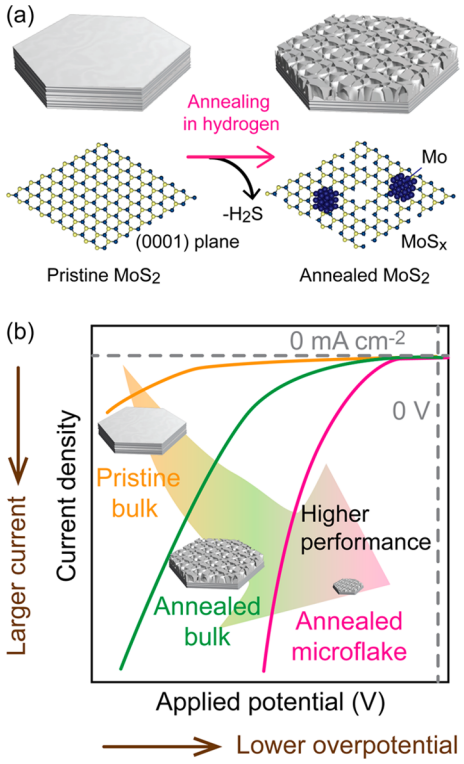

Figure 1. (a) Schematic illustration of the thermal texturization process of the (0001) plane of MoS_2. Annealing under a hydrogen environment generates H_2S through dissociation of the MoS_2 surface which increases the edge site density and generates Mo clusters. (b) Schematic illustration of the polarization (current density vs applied potential) curves for pristine bulk MoS_2, annealed bulk MoS_2, and annealed microflake MoS_2. The annealing process is expected to improve the HER performance (higher current density), more dramatically so for the microflake MoS_2.

the resistivity of the MoS_2 starting material by decomposing the MoS_2 into edge sites and forming Mo clusters on the surface. The work presents a general platform for using MoS_2 mineral as an efficient HER catalyst.

To generate the catalytic activity of the pristine bulk mineral MoS_2, the surface was intentionally dissociated as shown schematically in Figure 1a. Thermal annealing in a hydrogen environment is a straightforward dissociation process; sulfur atoms in MoS_2 would be removed as H_2S gas leading to the formation of vacancies and edges in the (0001) plane of the MoS_2. Simultaneously, the excess Mo forms metal clusters on the flake. It was hypothesized that this process could improve the HER activity of the bulk mineral MoS_2 by increasing the edge site density on the surface and by making the flake conductive through the generation of Mo clusters. Figure 1b shows schematically the expected results of increased HER performance for the annealed bulk MoS_2 as compared to the pristine bulk MoS_2. This thermal texturization strategy would be simple and effective, having universal applicability to not only bulk mineral MoS_2, but also to other MoS_2 morphologies with higher starting edge-to-surface ratios, such as micron-size MoS_2 flakes, to further improve HER activity (Figure 1b).

Figure 2 shows scanning electron microscope (SEM) images for bulk mineral MoS_2, micron-scale flakes (microflake), and mechanically ground micron-scale flakes of MoS_2 (ground microflake). As-received (i.e., no thermal damage) bulk MoS_2 shows smooth (0001) crystal planes (Figure 2a). Upon annealing at 700 °C in a forming gas (H_2/N_2 = 5%/95%) atmosphere for 3 h, the surface shows signs of dissociation thereby increasing the defect density, including edge sites, with the effect further increasing at 900 °C (Figure 2a). The as-received microflakes (Graphene Supermarket) were in powder form; thus, it was necessary to cast the powder into a film in order to test its HER activity. The microflake film was made by casting

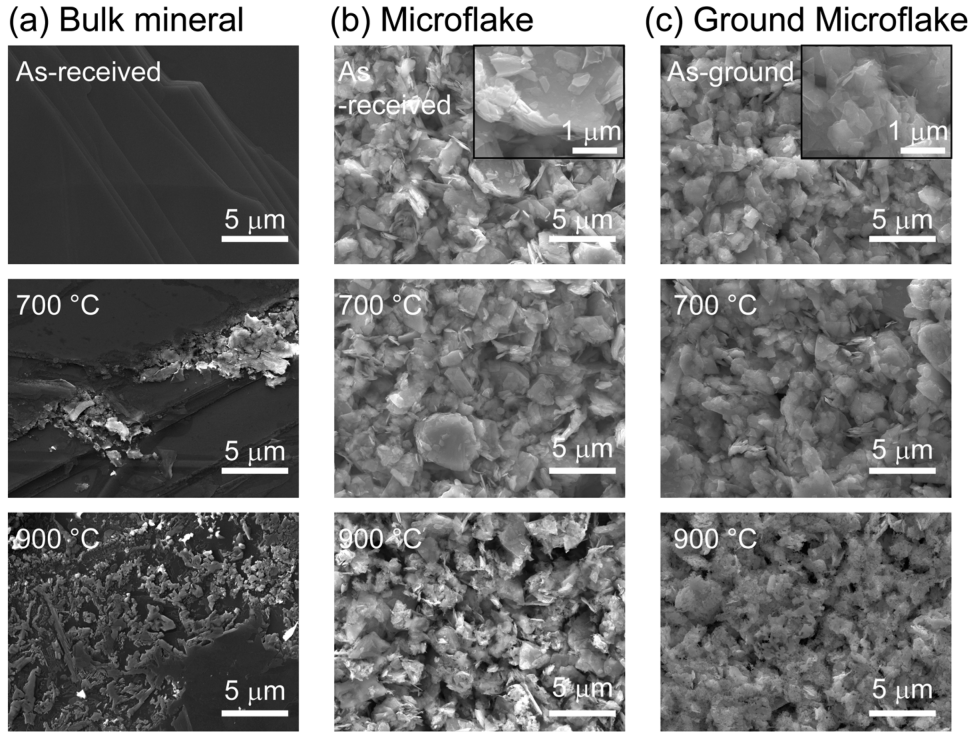

Figure 2. SEM images for (a) bulk mineral MoS_2, (b) microflake MoS_2, and (c) ground microflake MoS_2 after annealing at 250 °C (as-received or as-ground), 700 °C, and 900 °C for 3 h. The latter two microflake MoS_2 samples are both deposited as films on Mo foil.

DOI: 10.1021/acs.nanolett.6b00569
Nano Lett. XXXX, XXX, XXX−XXX

N,*N*-dimethylformamide (DMF) suspensions of the microflakes onto Mo foil. The film was then heated at 250 °C for 1 h to ensure all solvent was evaporated. The microflake film consists of flakes of ~2−5 μm in width (Figure 2b). The microflake films, annealed under the same conditions as the bulk mineral MoS_2, show a reduction in flake sizes, especially for the 900 °C annealing condition, again indicating an increase in the number of exposed edges. An additional method was used to attempt to make smaller MoS_2 flakes by grinding the as-received microflakes with a mortar and pestle. The as-prepared ground microflake film (as-ground) was cast into a film by the same procedure as the microflake film, and the same heat treatment was performed (Figure 2c). Further detail about the sample preparation can be found in the Supporting Information (SI).

In order to investigate how deep the apparent surface texturization extended into the MoS_2 flakes cross-sectional SEM images of the 900 °C annealed bulk MoS_2 were obtained (Figure 3a). It can be observed that the thermal texturization

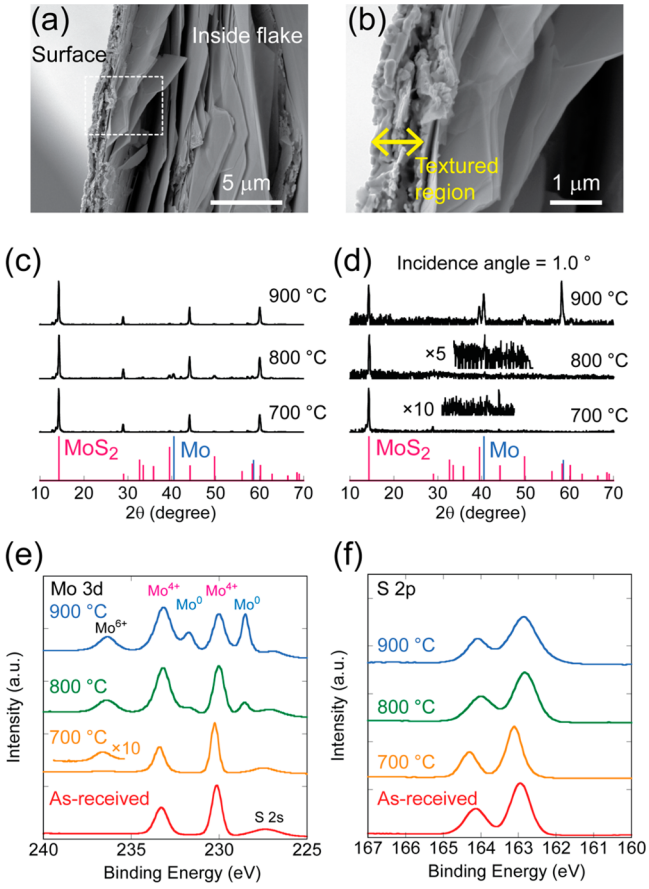

Figure 3. (a and b) Cross-sectional SEM images of annealed bulk MoS_2 at 900 °C for 3 h under a forming gas environment. (c) Powder XRD patterns for annealed bulk MoS_2 at 700 °C, 800 °C, and 900 °C with reference patterns for MoS_2 and Mo. (d) Grazing incident XRD (angle = 1°) for the same samples as in panel c. Increasing the annealing temperature induces stronger Mo signal at the surface. (e and f) XPS spectra for as-received and annealed bulk MoS_2 samples focused on the Mo 3d (e) and S 2p (f) regions. Increasing the annealing temperature induces an increase in the Mo^0 doublet signal, but all annealing conditions still show a sulfur signal.

penetrated about 1 μm into the flake after which the flake resembles the as-received bulk MoS_2 (smooth) (Figure 3b). This indicates that the dissociation occurs mainly at the surface exposed to hydrogen gas. X-ray diffraction (XRD) analysis shows the sample bulk remains as MoS_2 (Figure 3c). Surface-sensitive grazing angle XRD patterns indicate the presence of Mo on the surface (assumed to be clusters), with increasing Mo peak intensity as the annealing temperature is increased (Figure 3d). X-ray photoelectron spectroscopy (XPS) elucidates the surface elemental composition (Figures 3e and f). As-received bulk MoS_2 shows a doublet corresponding to Mo^{4+} $3d_{3/2}$ and $3d_{5/2}$ around 233 and 230 eV, respectively. The annealed samples show another doublet, which would correspond to Mo^0 $3d_{3/2}$ and $3d_{5/2}$ around 232 and 229 eV, respectively. The presence of Mo^0 indicates the generation of Mo on the surface. Moreover, the relative size of this Mo^0 doublet increases in comparison to the Mo^{4+} doublet with increasing annealing temperature, showing that the surface becomes increasingly Mo rich, in agreement with grazing angle XRD data. A peak due to Mo^{6+} is also observed in the annealed samples, which corresponds to the presence of MoO_3 in the near surface region. The presence of the oxide is thought to be due to thermally generated Mo^0 atoms which can be oxidized in air. Since MoO_3 dissolves in aqueous solutions, the MoO_3 would not affect the HER activity of the sample. Furthermore, sulfur 2p signals were observed around 163 eV in all annealed samples, indicating that the annealed samples maintain some MoS_2 at the surface even after annealing at 900 °C for 3 h. The valence band edges for the annealed MoS_2 flakes were also examined as shown in Figure S1. The flakes, after annealing at higher than 700 °C, show detectable density of states (DOS) around the Fermi level (at 0 eV). This DOS could potentially be from MoS_2 converted to the 1T metallic phase by hydrogen doping, but it is probable that the main contribution is from Mo nanoparticles on the surface, especially for the flakes annealed at 800 and 900 °C, where the reduced states are also clearly visible in the core level spectra.

To further investigate the crystalline structure of the catalyst surface, cross-sectional transmission electron microscopy (TEM) was performed on a texturized sample (700 °C). It was observed that the crystalline structure of the sample near the surface was similar to that observed several hundred nanometers deep in the same sample (Figure S2). Fast Fourier transform (FFT) analysis of the images show both regions to be highly crystalline, and all diffraction peaks obtained could be assigned to MoS_2, confirming that the MoS_2 structure remains near the surface after the hydrogen annealing treatment. Therefore, the MoS_2 crystalline structure has survived even at the surface after annealing at 700 °C for 3 h. At this temperature, there should be a small amount of texturization, and based off the grazing angle XRD and XPS, there should be a small amount of Mo metal near the surface. However, it is a well-known issue with cross-sectional TEM that imaging very near the sample surface is difficult due to platinum redeposition during the focused ion beam milling process. Thus, it is possible that these regions did exist on this sample, but it was not possible to observe them with the TEM done here.

To investigate the thermal texturization mechanism, SEM images of the bulk mineral MoS_2 were analyzed for three different annealing times (1, 3, and 5 h). As shown in Figure S3, the MoS_2 dissociation, which is observable as texturization of the surface, can be seen starting after 3 h of annealing. After 5 h of annealing, the dissociation on the surface is more obvious (Figure S3b). It can further be observed that the texturized areas have grown from defects and edges on the (0001) plane (Figure S3c). The texturization is arranged in a radial fashion,

DOI: 10.1021/acs.nanolett.6b00569
Nano Lett. XXXX, XXX, XXX−XXX

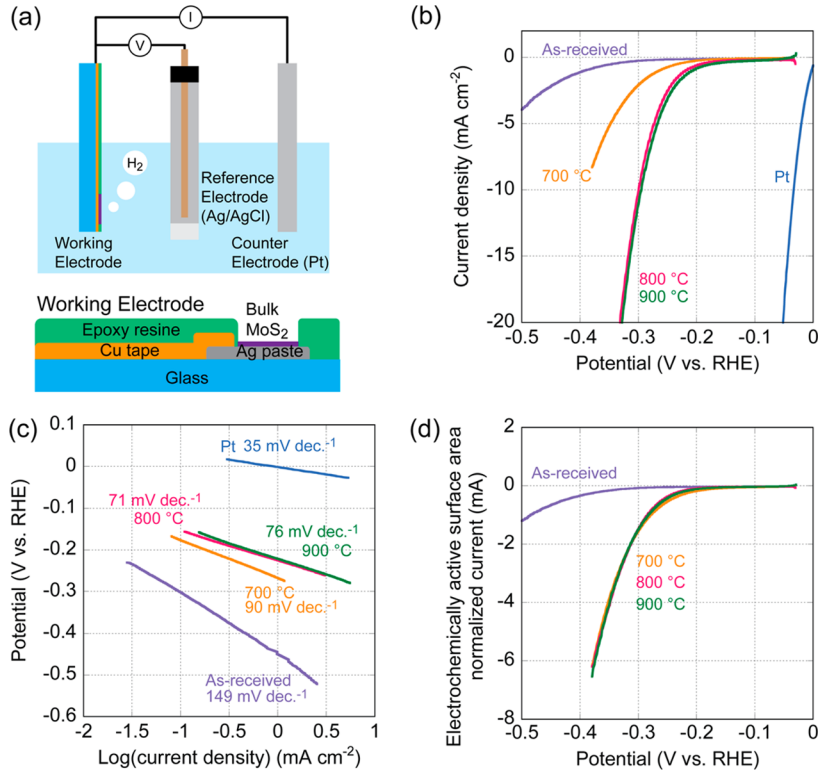

Figure 4. HER performance of the annealed bulk mineral MoS_2. (a) Illustration of the three electrode setup with a working electrode of bulk mineral MoS_2. (b and c) The polarization curves for as-received and annealed bulk samples (3 h under forming gas) and their corresponding Tafel plots. (d) Electrochemically active surface area normalized polarization curves from panel b. The three curves representing annealed samples from 700 to 900 °C fall onto the same curve, indicating the active sites for all three samples are similar. The similar tafel slopes from panel c corroborate this conclusion.

which indicates that the structure has grown from a defect. The surface texturization is only displayed when annealing in a hydrogen atmosphere and was not observed in a nitrogen atmosphere (Figure S4). After annealing in nitrogen at 800 °C, the surface is still macroscopically smooth, not rough like the samples annealed in forming gas. This difference would be explained because of the reaction between hydrogen and sulfur on the MoS_2 surface which is necessary to generate H_2S and dissociatively texturize the surface. In the nitrogen atmosphere, this reaction cannot occur, and thus sulfur atoms are not removed effectively from the surface and the texturization does not occur.[25]

The effect of thermal texturization can be monitored in metal-oxide semiconductor field-effect transistors (MOSFETs) as well. MOSFETs were fabricated with a standard photolithography process for mechanically exfoliated MoS_2 flakes (~100 nm in thickness) which were placed on a p^+-Si substrate with 260 nm SiO_2. The flakes were annealed under different conditions and then fabricated into the same device structure with a 10 μm channel length. As-received MoS_2 showed gate dependency of the drain current, as did low-temperature annealed MoS_2 (forming gas at 550 °C) (Figure S5a,b). This behavior indicates that the carrier concentration of these samples can be modulated electrostatically. On the other hand, the sample annealed at 700 °C in forming gas showed no gate dependency (Figure S5d), indicating the metallic state of the material, due most likely to the generation of Mo clusters. The sample annealed in nitrogen at 700 °C still shows a gate dependency (Figure S5c). These findings again support the importance of hydrogen to the effective dissociative texturization of the MoS_2.

The HER activity of the samples (see SI for sample preparation details) was analyzed with a common three electrode setup using a 0.5 M H_2SO_4 electrolyte, as shown in Figure 4a. All curves presented here were corrected for the voltage drop due to solution resistivity (IR drop), measured before each run via electrochemical impedance spectroscopy (EIS). Figure 4b shows the polarization curves for the bulk mineral MoS_2. The as-received bulk MoS_2 shows current density $j < 5$ mA cm^{-2} even up to −0.5 V vs the reversible hydrogen electrode (RHE) due to the dominant (0001) surface plane and the low density of active edge sites. In contrast, the forming gas annealed bulk MoS_2 shows fair HER performance with higher current densities at lower overpotentials. The Tafel plots for the bulk MoS_2 samples are shown in Figure 4c. The annealed samples show similar Tafel slope values of 70−90 mV decade^{-1}, which indicates the hydrogen evolution mechanism is similar for these samples. We further analyzed the HER performance of each sample by considering the electrochemically active surface area normalization. EIS measurements were applied to evaluate the relative active surface area for each bulk MoS_2 sample as shown previously[17] (see SI for method detail). Figure 4d shows the polarization curves normalized to electrochemically active surface area. All of the curves for the annealed samples fall onto a similar line, meaning the forming gas dissociation process generates similar active sites on the surface with the main difference between samples annealed at different temperatures being the density of surface sites generated, thus explaining the changes in $j-V$ behavior in Figure 4b.

To demonstrate the effectiveness of this thermal texturization approach to generate catalytic HER performance with other

DOI: 10.1021/acs.nanolett.6b00569
Nano Lett. XXXX, XXX, XXX−XXX

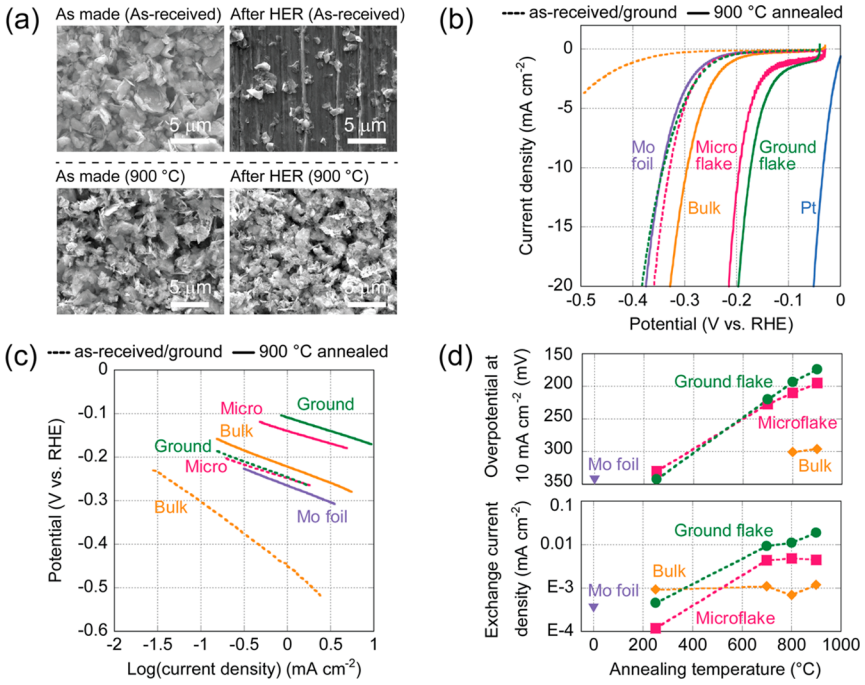

Figure 5. Improvement of HER performance for the microflake/ground microflake MoS_2 films by the thermal texturization process. (a) SEM images of the as-received and 900 °C annealed microflake MoS_2 films on Mo foil before (as made) and after hydrogen generation. The as-received film shows delamination. (b) The polarization curves for the bulk, microflake, and ground microflake films of MoS_2 as-received or as-ground (dot line) and annealed at 900 °C (solid line). As-received and as-ground microflake films were evaluated after delamination. The scan rate was 50 mV s^{-1}. Curves for bulk mineral MoS_2 are identical to Figure 4b. (c) Tafel plots for the bulk, microflake, and ground microflake films as-received/as-ground and annealed at 900 °C. Curves for the bulk mineral MoS_2 are identical to Figure 4c. (d) (Top) Overpotential required to obtain a current density of 10 mA cm^{-2} for each sample. All MoS_2 samples (bulk, microflake, and ground microflake) show a corresponding decrease in the required overpotential with increasing annealing temperature. Samples annealed at 250 °C correspond to the as-received or as-ground sample. Both as-received and 700 °C annealed bulk MoS_2 did not show 10 mA cm^{-2} within the range measured. The values for the as-received and as-ground microflake films are after delamination. (Bottom) Plot of exchange current density vs annealing temperature. Decreasing the flake size from bulk to ground microflake, the exchange current density increases.

MoS_2 materials, we applied it to microflake and ground microflake films. Microflakes and ground microflakes have larger edge-to-body ratios than bulk mineral MoS_2 (Figure 2); therefore, they have a higher realizable catalytic performance. We found that the as-received microflake and as-ground microflake MoS_2 films (annealed at 250 °C in the forming gas) are difficult to operate in HER experiments; once hydrogen bubbles are generated, the films easily delaminate from the substrate (Figures 5a and S6). It is difficult to keep the films on the substrate, making it difficult to use as a catalyst in a film configuration on a conductive substrate. On the other hand, annealed samples did not delaminate from the surface (Figure 5a), although some partial flaking off could occur. Therefore, for microflake and ground microflake MoS_2 samples the annealing process is useful toward making an effective HER catalyst.

Figure 5b shows polarization curves for bulk, microflake, and ground microflake films of MoS_2 annealed at 250 °C (as-received/as-ground, dotted) and 900 °C (solid). As-received and as-ground microflake films produce similar curves to Mo foil because of the large amount of delamination that occurred with these films. The annealed samples, however, show a clear trend: a monotonic increase in current density with decreasing flake size. This trend can be explained as an increasing relative number of edge sites due to the shrinking size of the flakes. The Tafel slopes of the annealed micro and ground microflakes samples are ~60−70 mV $decade^{-1}$ (Figures 5c, S6, S7, and Table S1). The mechanism of hydrogen adsorption/desorption is similar in these cases and the Tafel slope value is close to the Heyrovsky reaction regime (40 mV $decade^{-1}$), indicating that the rate-limiting step here is the electrochemical desorption step (see SI for further details).

Two important parameters used to evaluate the HER activity of a sample are the magnitude of the required overpotential and the exchange current density (j_0).[26,27] A common way of evaluating the required overpotential is to report the overpotential (η) needed to obtain 10 mA cm^{-2} (Figure 5d).[27] For all cases, η monotonically decreases from as high as 342 mV to as low as 174 mV as the sample's annealing temperature increases (Figure 5d and Table S1), showing that the thermal texturization is effective for all sample morphologies. The exchange current density was also evaluated and is shown in Figure 5d. It can be seen that decreasing the flake size, from bulk to microflake to ground microflake, increased j_0 from ~10^{-3} mA cm^{-2} (bulk) to ~0.019 mA cm^{-3} (ground microflake) in the 900 °C annealing case. It is important to note here that the as-received/as-ground microflake films were evaluated after delamination had completely stopped (surface similar to that shown in Figure 5a after HER); thus, it is not surprising that the overpotential to reach 10 mA cm^{-2} and the j_0 for these samples are similar to Mo foil which is the underlying substrate. Finally, the long-term stability of the MoS_2 microflake film annealed at 900 °C was examined by a chronoamperometry measurement (j−t). The electrolysis measurement was performed for more than 12 h at a constant potential, and a current density of about 12 mA cm^{-2} was maintained (Figure S6).

DOI: 10.1021/acs.nanolett.6b00569
Nano Lett. XXXX, XXX, XXX−XXX

We further demonstrate the wide-range of applicability of this thermal texturization process by applying it to a commercially available spray of MoS_2 (CRC company), for which the intended application is lubrication. The MoS_2 spray was applied to a Mo foil, as shown in Figure 6a, and was found

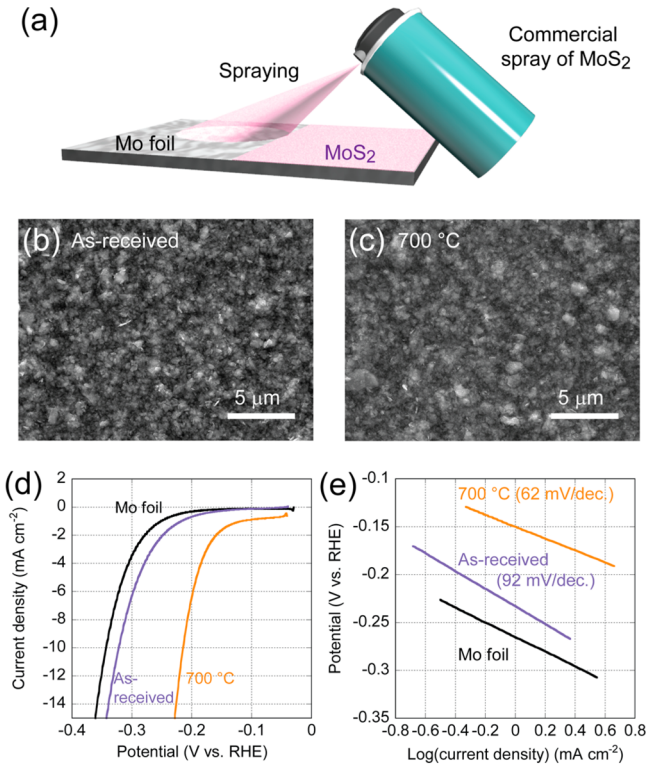

Figure 6. (a) Schematic illustration of the preparation process for a film made from a commercially available spray lubricant containing MoS_2. (b, c) SEM images of the as-received (b) and 700 °C annealed (c) sprayed films. Nanoflakes (~200 nm width) were observed. Polarization curves (d) and Tafel plots (e) for the as-received sprayed nanoflake film, 700 °C annealed sprayed MoS_2 films, and Mo foil (which is the underlying substrate).

to be composed of nanosized flakes of MoS_2 with ~200 nm size under SEM (Figures 6b,c). After annealing in forming gas at 700 °C, the overpotential at 10 mA cm^{-2} decreased from 322 mV to 215 mV, a ~100 mV drop (Figure 6d and Table S1). Furthermore, the makeup of the spray helped adhere the film to the Mo foil substrate even for the as-received case (250 °C heated). Thus, unlike the previous cases, the relative comparison between as-received and 700 °C annealed is reasonable. The Tafel slopes for the as-received sprayed MoS_2 and the annealed sample are 92 and 62 mV $decade^{-1}$, respectively (Figure 6e). The decrease in the Tafel slope is substantial and brings it close to the value observed for the microflake films above. From all the results presented here, we believe our thermal texturization method could be applied to all MoS_2 materials and could be effective to further improve already high performance synthesized MoS_2 catalysts.

In summary, we have demonstrated a simple method to generate or improve the catalytic HER performance of MoS_2 by thermal texturization. The process involves a simple thermal annealing in a hydrogen environment and is applicable to a wide range of MoS_2 morphologies, such as bulk and microflakes. The overpotential required to obtain 10 mA cm^{-2} can be decreased as low as 174 mV for the ground microflake film case. The method is further applicable to a commercially available MoS_2 lubricant spray, which shows more than a 100 mV decrease in required overpotential as compared to the as-received MoS_2 spray. This indicates the universality of this method to improve MoS_2 HER performance as well as its potential to be a scalable production method with a cheap material. Moreover, this method relies on removing the atoms from the chalcogen sites to generate edges on MoS_2, and it could be still more widely applicable to other 2D materials, such as WS_2, as a means to activate/improve their catalytic properties.[28,29]

■ ASSOCIATED CONTENT

Supporting Information

The Supporting Information is available free of charge on the ACS Publications website at DOI: 10.1021/acs.nanolett.6b00569.

Detailed sample preparation and characterizations, electrochemical parameters, XPS spectra of the valence band edge, analysis of the mechanism of the thermal texturization, annealing environmental effect for HER performance, electrical characterization of annealed samples, electrochemical data for microflake and ground microflake MoS_2 films (PDF)

■ AUTHOR INFORMATION

Corresponding Author

*E-mail: ajavey@berkeley.edu.

Author Contributions

D.K. and P.L. contributed equally.

Notes

The authors declare no competing financial interest.

■ ACKNOWLEDGMENTS

XPS, SEM, XRD, and the final electrochemical characterization work was performed in collaboration with the Joint Center for Artificial Photosynthesis (JCAP), a DOE Energy Innovation Hub, supported through the Office of Science of the U.S. Department of Energy under Award Number DE-SC0004993. Processing and initial electrochemical characterization were performed in the Electronic Materials Program, which is supported by Director, Office of Science, Office of Basic Energy Sciences, Materials Sciences and Engineering Division, of the U.S. Department of Energy under Contract No. DE-AC02-05CH11231. TEM work was performed in collaboration with Mary Scott at the Molecular Foundry, which is supported by the Office of Science, Office of Basic Energy Sciences, of the U.S. Department of Energy under Contract No. DE-AC02-05CH11231.

■ REFERENCES

(1) Chu, S.; Majumdar, A. *Nature* **2012**, *488*, 294−303.
(2) Cook, T. R.; Dogutan, D. K.; Reece, S. Y.; Surendranath, Y.; Teets, T. S.; Nocera, D. G. *Chem. Rev.* **2010**, *110*, 6474−6502.
(3) Walter, M. G.; Warren, E. L.; McKone, J. R.; Boettcher, S. W.; Mi, Q.; Santori, E. A.; Lewis, N. S. *Chem. Rev.* **2010**, *110*, 6446−6473.
(4) Lewis, N. S.; Nocera, D. G. *Proc. Natl. Acad. Sci. U. S. A.* **2006**, *103*, 15729−15735.
(5) Gray, H. B. *Nat. Chem.* **2009**, *1*, 7.
(6) Kong, D.; Wang, H.; Lu, Z.; Cui, Y. *J. Am. Chem. Soc.* **2014**, *136*, 4897−4900.
(7) Crabtree, G. W.; Dresselhaus, M. S.; Buchanan, M. V. *Phys. Today* **2004**, *57*, 39−44.
(8) Turner, J. A. *Science* **2004**, *305*, 972−974.

DOI: 10.1021/acs.nanolett.6b00569
Nano Lett. XXXX, XXX, XXX−XXX

(9) Hinnemann, B.; Moses, P. G.; Bonde, J.; Jørgensen, K. P.; Nielsen, J. H.; Horch, S.; Chorkendorff, I.; Nørskov, J. K. *J. Am. Chem. Soc.* **2005**, *127*, 5308−5309.
(10) Lu, Q.; Yu, Y.; Ma, Q.; Chen, B.; Zhang, H. *Adv. Mater.* **2016**, *28*, 1917−1933.
(11) Ng, J. W. D.; Hellstern, T. R.; Kibsgaard, J.; Hinckley, A. C.; Benck, J. D.; Jaramillo, T. F. *ChemSusChem* **2015**, *8*, 3512−3519.
(12) Jaramillo, T. F.; Jørgensen, K. P.; Bonde, J.; Nielsen, J. H.; Horch, S.; Chorkendorff, I. *Science* **2007**, *317*, 100−102.
(13) Karunadasa, H. I.; Montalvo, E.; Sun, Y. J.; Majda, M.; Long, J. R.; Chang, C. J. *Science* **2012**, *335*, 698−702.
(14) Xie, J.; Zhang, H.; Li, S.; Wang, R.; Sun, X.; Zhou, M.; Zhou, J.; Lou, X. W.; Xie, Y. *Adv. Mater.* **2013**, *25*, 5807−5813.
(15) Li, Y.; Wang, H.; Xie, L.; Liang, Y.; Hong, G.; Dai, H. *J. Am. Chem. Soc.* **2011**, *133*, 7296−7299.
(16) Liao, L.; Zhu, J.; Bian, X.; Zhu, L.; Scanlon, M. D.; Girault, H. H.; Liu, B. *Adv. Funct. Mater.* **2013**, *23*, 5326−5333.
(17) Kibsgaard, J.; Chen, Z. B.; Reinecke, B. N.; Jaramillo, T. F. *Nat. Mater.* **2012**, *11*, 963−969.
(18) Zhang, Y.; Zuo, L.; Huang, Y.; Zhang, L.; Lai, F.; Fan, W.; Liu, T. *ACS Sustainable Chem. Eng.* **2015**, *3*, 3140−3148.
(19) Wang, H.; Lu, Z.; Xu, S.; Kong, D.; Cha, J. J.; Zheng, G.; Hsu, P.-C.; Yan, K.; Bradshaw, D.; Prinz, F. B.; Cui, Y. *Proc. Natl. Acad. Sci. U. S. A.* **2013**, *110*, 19701−19706.
(20) Lu, Z.; Zhu, W.; Yu, X.; Zhang, H.; Li, Y.; Sun, X.; Wang, X.; Wang, H.; Wang, J.; Luo, J.; Lei, X.; Jiang, L. *Adv. Mater.* **2014**, *26*, 2683−2687.
(21) Yang, Y.; Fei, H.; Ruan, G.; Li, Y.; Tour, J. M. *Adv. Funct. Mater.* **2015**, *25*, 6199−6204.
(22) Voiry, D.; Salehi, M.; Silva, R.; Fujita, T.; Chen, M.; Asefa, T.; Shenoy, V. B.; Eda, G.; Chhowalla, M. *Nano Lett.* **2013**, *13*, 6222−6227.
(23) Lukowski, M. A.; Daniel, A. S.; Meng, F.; Forticaux, A.; Li, L.; Jin, S. *J. Am. Chem. Soc.* **2013**, *135*, 10274−10277.
(24) Ambrosi, A.; Sofer, Z.; Pumera, M. *Chem. Commun.* **2015**, *51*, 8450−8453.
(25) Liu, D.; Chen, X.; Li, D.; Wang, F.; Luo, X.; Yang, B. *J. Mol. Struct.* **2010**, *980*, 66−71.
(26) Zheng, Y.; Jiao, Y.; Jaroniec, M.; Qiao, S. Z. *Angew. Chem., Int. Ed.* **2015**, *54*, 52−65.
(27) Benck, J. D.; Hellstern, T. R.; Kibsgaard, J.; Chakthranont, P.; Jaramillo, T. F. *ACS Catal.* **2014**, *4*, 3957−3971.
(28) Cheng, L.; Huang, W.; Gong, Q.; Liu, C.; Liu, Z.; Li, Y.; Dai, H. *Angew. Chem., Int. Ed.* **2014**, *53*, 7860−7863.
(29) Lukowski, M. A.; Daniel, A. S.; English, C. R.; Meng, F.; Forticaux, A.; Hamers, R. J.; Jin, S. *Energy Environ. Sci.* **2014**, *7*, 2608−2613.

DOI: 10.1021/acs.nanolett.6b00569
Nano Lett. XXXX, XXX, XXX−XXX